A Matching Algorithm for Detecting Land Use Changes Using Case-Based Reasoning

Xia Li, Anthony Gar-On Yeh, Jun-ping Qian, Bin Ai, and Zhixin Qi

Abstract

The paper deals with change detection using time series SAR images. SAR provides a unique opportunity for detecting land-use changes within short intervals (e.g., monthly) in tropical and sub-tropical regions with cloud cover. Traditional change detection methods mainly rely on per-pixel spectral information but ignore per-object structural information. In this study, a new method is presented that integrates object-oriented analysis with case-based reasoning (CBR) for change detection. Object-oriented analysis is carried out to retrieve a variety of features, such as tone, shape, texture, area, and context. An incremental segmentation technique is proposed for deriving change objects from multi-temporal Radarsat images. Feature selection based on genetic algorithms is carried out to determine the optimal set of features for change detection. A CBR matching algorithm is developed to identify the temporal positions and the kind of changes. It is based on the weighted k-Nearest Neighbor classification using an accumulative similarity measure. The comparison of the four combinations of change detection methods, object-based or pixel-based plus case-based or rule-based, is carried out to validate the performance of this proposed method. The analysis shows that this integrated approach has provided an efficient way of detecting land-use changes at monthly intervals by using multi-temporal SAR images.

Introduction

Since the launch of ERS-1 (1991) and ERS-2 (1995) by the European Space Agency (ESA) and Radarsat-1 (1995) by the Canadian Space Agency (CSA) and NASA, the synthetic aperture radar (SAR) has become a weather-independent monitoring tool covering a large part of the globe on a regular basis. There is an increasing demand for using satellite SAR images as a complementary data source for resource inventory and environmental monitoring (Ranson and Sun, 2000; Baghdadi *et al*., 2001; Magagi *et al*., 2002). This is because conventional optical remote sensing may have difficulties in collecting the desired ground data in regions frequently affected by clouds; hence, it cannot be used for monitoring land-use changes, especially for identifying illegal land development in fast-growing regions in tropical and sub-tropical areas that often experience cloud cover. Monitoring land-use changes in these areas on a regular basis (e.g., monthly) can help to prevent illegal developments at an early stage. Monthly SAR images can obtain ground information almost in real time and thereby provide an efficient tool for monitoring land-use changes and urban development in rapidly developing regions.

Monitoring land-use changes at short intervals can be based on the independent classification of these monthly SAR images. Post-classification comparison can be used to identify not only the amount and location of change but also the nature of change (Howarth and Wickware, 1981; Richards and Jia, 1999). However, such comparison has limitations because the classifications of individual images always contain errors and the resulting change-detection analysis can end up being more a classification of error than a classification of change. As a result, the degree of land-use changes may be overestimated by comparing a number of independent classifications (Li and Yeh, 1998). Moreover, this type of method faces difficulties when a long sequence of time series data is involved. A common method is to apply principal components analysis (PCA) to obtain information on land-use changes from a long sequence of time series data (Eastman and Fulk, 1993; Li and Yeh, 1998).

Although many studies exist on the methodologies of change detection, only a few have been devoted to change detection using SAR images, mainly because of the intrinsic complexity of SAR data. Recently, some studies have been published on the development of algorithms using SAR images for change detection (Bovolo and Bruzzone, 2005). However, there is still a general lack of studies that focus on the use of object-oriented analysis to retrieve spatial information from SAR images for change detection.

Orbital radar images are at present often obtained using only one single frequency (e.g., C-band). Significant confusion arises if land-use classification and change detection are based purely on the information of a single band of these SAR data (Li and Yeh, 2004). The first way to reduce such confusion is to use time series SAR images, since temporal information can partially compensate for the limitations of using a single frequency. The second way is to derive ancillary features related to structural information,

Xia Li and Bin Ai are with the School of Geography and Planning, Sun Yat-sen University, 135 West Xingang Rd., Guangzhou 510275, P.R. China (lixia@mail.sysu.edu.cn; lixia@graduate.hku.hk).

Anthony Gar-On Yeh and Zhixin Qi are with the Centre of Urban Planning and Environmental Management, The University of Hong Kong, Pokfulam Road, Hong Kong SAR, P.R. China.

Jun-ping Qian is with the School of Geography and Planning, Sun Yat-sen University, 135 West Xingang Rd., Guangzhou 510275, P.R. China, and the Guangzhou Institute of Geography, Guangzhou 510070, PR China.

such as texture and shape, in addition to the backscatter. Object-oriented analysis can be applied to radar images to obtain this type of structural information. Such analysis is especially useful for improving the classification accuracy of high-resolution images (Langford, 2002). Although textural and contextual information have been used for classifying SAR images, these analyses are purely pixel-based approaches and have limitations for representing objects in high-resolution images. Object-oriented image approaches can obtain a variety of additional spatial information, which is crucial for improving the accuracy of remote sensing classification (Benz *et al*., 2004). These approaches can extract information on tone, shape, texture, area, context, and their spatial relationships based on image objects.

Rule-based techniques have been used in the classification of radar images (Dobson *et al*., 1996). Pierce *et al*. (1998) also found that the same rules developed in previous studies can be applied to other studies for a time-independent classification of land-cover. However, a well-known problem in creating expert systems is the "knowledge acquisition bottleneck" (Huang and Jensen, 1997). The process of acquiring domain knowledge is tedious and time consuming. For example, McAvoy and Krakowski (1989) used approximately 100 rules to classify ice floes into different "age" categories using SAR images.

Case-based reasoning (CBR) techniques can be used to solve these knowledge solicitation problems. These techniques have the advantages inherited from knowledge-based systems, such as artificial intelligence, reduction of repetitive tasks, and highly automated capability. They do not require rules to be elicited from past experiences and can save time in soliciting knowledge on change detection using multi-temporal images. Studies have also shown that the CBR method can even provide better accuracy of classification than traditional statistical methods (Watson, 1997). It has many applications in engineering, medicine, and business (Watson, 1997) and has also recently been used to solve problems in the fields of environmental science, urban planning, and geography (Branting and Hastings, 1994; Lekkas *et al*., 1994; Yeh and Shi, 1999).

This study will develop the methodology of detecting short-interval land development by using multi-temporal SAR images. The proposed method is based on the integration of object-oriented analysis with CBR. First, an incremental segmentation procedure is proposed to remove the uncertainties in object delineation by using multi-temporal SAR images. Object-oriented analysis serves two main purposes: delineating objects (land parcels) and calculating various features of each object for CBR. Then, genetic algorithms are used to select an optimal subset of the features created from the object-oriented analysis. Finally, a CBR matching algorithm is developed for detecting spatio-temporal land-use changes in multi-temporal SAR images. The proposed method uses discrete cases to capture complex relationships in order to infer land-use changes.

Study Area and Data
The study area is situated in the Panyu District of Guangzhou in southern China. Panyu, a densely populated area at the center of the Pearl River Delta (Figure 1), has a total land area of 1,314 km^2 and a population of 926,542. This district was an agricultural county before economic reform in 1978 but has been transformed recently into a rapidly urbanized area. The land-use types include built-up areas, rural residential areas, bare land, paddy fields, vegetable land, orchards, forest, river, and fishponds.

Intensive land development has occurred since Panyu became a district of Guangzhou in July 2000. A major type of land development is related to the property market, which provides housing to the residents of Guangzhou City. Huge profits have been generated through property development, resulting in the increase of land speculation activities and illegal land development. Weak regulations have led to many unreported development sites in the study area. The environment may experience substantial irreversible damage if no early warning system is available to monitor illegal land development at regular short intervals.

Monthly Radarsat images with the fine-mode (Fine 4 Far) and Single Look Complex (SLC) from 20 September 2005 to 31 August 2006 were used to monitor short-interval land development in the study area. Radarsat-1 provided horizontal-transmit and horizontal-receive (HH) data only. These SAR images had a resolution of 4.6 m × 5.1 m and a swath width of 50 km on the ground. The incidence angle was about 45°. One scene of Radarsat images can cover the majority of the Panyu area.

The acquisition dates for these SAR images are listed in Table 1. A SPOT-5 image (2.5 m panchromatic and 10 m multispectral bands) dated 06 January 2005 was acquired to assist the collection of ground true information. GPS was used to record the positions of ground-collected data (e.g., land-use and land-use changes), and the cases of stable land-use types (non-changes) were stored in the case library.

Radiometric calibration of the SAR data was carried out using the Radar Analysis Package of the PCI software. Calculating the backscattering value of each pixel involves

Figure 1. The study area for detecting fast land-use changes in the Pearl River Delta.

TABLE 1. ACQUISITION DATES FOR THE TIME SERIES OF RADARSAT IMAGES

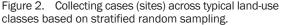| No.	Acquisition time	No.	Acquisition time
1	*20 Sep 2005*	**9**	*09 Apr 2006*
2	*23 Oct 2005*	**10**	*03 May 2006*
3	*16 Nov 2005*	**11**	*27 May 2006*
4	*10 Dec 2005*	**12**	*20 Jun 2006*
5	*03 Jan 2006*	**13**	*14 Jul 2006*
6	*27 Jan 2006*	**14**	*07 Aug 2006*
7	*20 Feb 2006*	**15**	*31 Aug 2006*
8	*16 Mar 2006*		

three procedures: (a) converting the pixel DN values into the slant range backscattering coefficient (Beta Nought) using the scaling and gain coefficients in the raw data, (b) calculating the incidence angle for each pixel of the images in the range direction, and (c) incorporating the incidence angle to extract the Radarsat backscatter coefficient (Sigma Nought) from the Beta Nought values.

Image registration was then implemented using the AutoSync component of the ERDAS software. This component provides the Automatic Point Measurement (AMP) tool for finding the control points, which are used to register these SAR images. A second order polynomial model was applied by transforming these SAR images. The average RMS error was below 0.5 pixel for the transformation.

SAR images are often affected by a kind of noise called speckle. Therefore, speckle reduction techniques were employed to minimize this noise effect before carrying out image segmentation. The gamma map filter (GMF) was used to remove high-frequency noise (speckle) while preserving high-frequency features (edges) for SAR images. Through shape adaptive windowing, GMF detectors allow the use of large window sizes for better speckle reduction while preserving spatial resolution and structural features (Lopes *et al.*, 1993). Following speckle reduction, these SAR data were resampled to 6.25 m × 6.25 m.

Field investigation was carried out to obtain the spatial data for three purposes: (a) determining the optimal features using genetic algorithms (GA), (b) establishing the case library for change detection, and (c) verifying the results of land-use classification and change detection. A total of 418 cases (sites) were selected across typical land-use classes (initial land-use types) based on stratified random sampling (Congalton, 1991) (Figure 2). The dates for the field investigation are close to those of the acquired Radarsat images so that true land-use types are obtained for these cases. The

main attribute collected in the field is land-use type at each site. GPS was used to record the coordinates of these sites. These collected cases were divided into two groups for training and validation: 265 cases for training and 153 cases for validation (Figure 2 and Table 2). The first data set was used to determine the optimal features in GA and to establish the case library. The second data set was used to verify the results of land-use classification and change detection.

Object-oriented Analysis and Feature Selection

Incremental Segmentation for Deriving Change Objects

Object-oriented analysis can be applied to radar images to obtain this type of structural information. Such analysis is especially useful in improving the classification accuracy of high-resolution images (Langford, 2002; Champagne *et al.*, 2006; Chubey *et al.*, 2006). The first step of the object-oriented analysis is to extract land parcels (homogenous objects) in the SAR images. The image segmentation is implemented by using the functions provided by the object-oriented package, eCognition® (Baatz *et al.*, 2004). The delineation of homogenous objects is based on shape and spectral homogeneity (Uchiyama and Arbib, 1994; Grund, 2003). A heuristic optimization procedure is used to minimize the average heterogeneity of image objects for a given resolution over the whole scene during the multivariate segmentation (Baatz and Schäpe, 2000). Heterogeneity is based not only on the standard deviation of spectral properties but also on their shapes. Both spectral and shape heterogeneity are used to adjust the segmentation in order to obtain the best discrimination effects.

This segmentation is a bottom-up approach that uses a region-merging technique starting with one-pixel objects. During the region-merging process, smaller image objects are merged into bigger ones. The optimization procedure is used to minimize the heterogeneity of the resulting image objects.

In this study, a suitable fixed scale was used to segment objects. Some experiments were carried out to determine the optimal scale for the segmentation. The scale parameter is a measure for the maximum change in heterogeneity that may occur when merging two image objects. Internally, this value is squared and serves as the threshold that terminates the segmentation algorithm. Adjusting the so-called scale parameter indirectly influences the average object size, i.e., a larger value leads to bigger objects and vice versa.

Figure 3 shows the corresponding segmentation results related to the segmentation parameters of various scales (Table 3). The segmentation of Radarsat images with a scale of 20 was found to best fit the land parcels in the SPOT image. Figure 3b shows the results by overlaying the boundaries of the segmented Radarsat image with scale = 20 on the SPOT image.

The next step was to derive the change objects in the multi-temporal SAR images using scale = 20. Some modifications were adopted for applying the above segmentation techniques to derive change objects. There are two ways to segment multi-temporal satellite images. A straightforward method is to segment these images separately and then overlay them together. These separate segmentations will

Figure 2. Collecting cases (sites) across typical land-use classes based on stratified random sampling.

○ Training cases   ▲ Validation cases

TABLE 2. TRAINING AND VALIDATION DATA OF VARIOUS LAND-USE TYPES IN THE STUDY AREA

Land-use types	River	Fishpond	Paddy	Vegetable	Orchard	Forest	Bare land	Built-up	Rural residential	*Total*
Training	24	28	28	35	28	26	32	33	31	***265***
Validation	14	16	16	20	16	15	18	19	18	***153***

Figure 3. Determining the optimal scale for segmentation of Radarsat images: (a) Multi-scale segmentation, and (b) Land parcels in SPOT image.
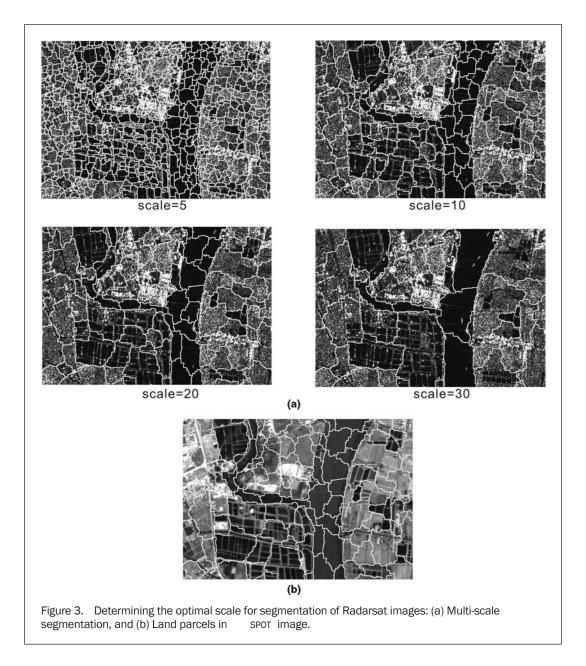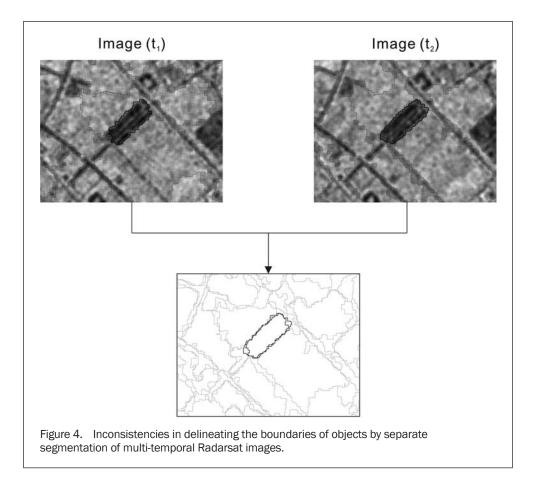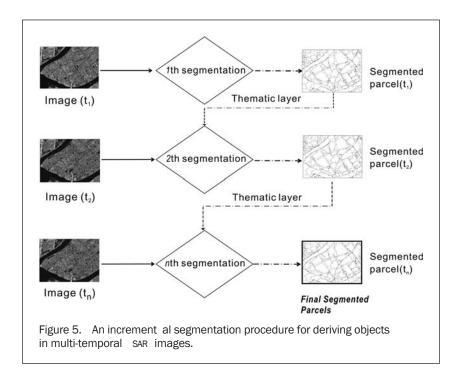
TABLE 3. SEGMENTATION PARAMETERS OF VARIOUS SCALES (REFERENCING "ECOGNITION PROFESSIONAL 4.0 USER GUIDE" FOR THE PARAMETERS)

Segmentation	Scale parameter	Tone w_{tone}	Shape w_{shape}	Compactness $w_{compact}$	Smoothness w_{smooth}
1	30	0.75	0.25	0.9	0.1
2	20	0.75	0.25	0.9	0.1
3	10	0.75	0.25	0.9	0.1
4	5	0.75	0.25	0.9	0.1

produce inconsistencies in delineating the boundaries of objects, resulting in a large number of objects (patches) in the final segmented image (Figure 4). In addition, there is an exponential increase of patches as more sequential images are included in the change detection. This excessive fragmentation can bring about difficulties in change detection. In particular, this study involves 15 Radarsat images for the segmentation.

An incremental segmentation procedure is proposed to minimize the inconsistency of object delineation in temporal images (Figure 5). The incremental delineation of objects at $t + 1$ is based on the segmentation result at t. The detailed procedure is as follows:

1. The initial segmentation with a fixed scale parameter (e.g., $f = 20$) is applied to image (t) based on the principle

Figure 4. Inconsistencies in delineating the boundaries of objects by separate segmentation of multi-temporal Radarsat images.

Figure 5. An increment al segmentation procedure for deriving objects in multi-temporal SAR images.

of minimizing the spectral heterogeneity and shape heterogeneity. This segmented image is treated as the thematic layer for the next step of segmentation in the eCognition® software.

2. Image (t) is substituted with image ($t + 1$) and the segmentation is run again. The same scale parameter is applied to the segmentation of image ($t + 1$) while the result of Step 1 is taken as the thematic layer for constraint. With the constraint

of the previous segmentation, all the object-merging will take place only within the boundaries of the image (*t*) segmentation. No objects that reach beyond the border of a polygon or are larger than such a polygon in the thematic layer will be created if the thematic layer is incorporated. Moreover, this segmentation will only create new objects in the places where the image (*t* + 1) is significantly different from image (*t*).

3. The segmentation result of image (*t* + 1) is compared with that of image (*t*) to find the new objects, which are created from the segmentation of image (*t* + 1) and do not exist in the segmentation result of image (*t*).
4. This new segmented image is then treated as the new thematic layer. The Steps from 1 to 3 will continue until all the temporal images have been processed for this incremental segmentation.

This incremental segmentation can effectively avoid the inconsistency in separate segmentations by using multi-temporal images. It generates homogenous objects according to the factors of the spectral and shape heterogeneity. There are two major types of these objects: (a) stable objects without land-use changes, and (b) objects with land-use changes. In this study, various textural and shape features were extracted from each object after these multi-temporal SAR images were segmented. The object-oriented analysis created a total of 86 features, which include the following four major categories:

- 6 indicators related to the statistical values of each object (e.g., min, max, mean, and standard deviation of backscatter);
- 11 indicators related to spatial relationship (e.g., mean difference to neighbors and mean difference to brighter neighbors);
- 57 indicators related to shape (e.g., area, length, number of segments, and curvature/length); and
- 12 indicators related to texture (e.g., GLCM Homogeneity, GLCM Contrast, GLCM Dissimilarity, and GLCM Entropy).

Feature Selection using Genetic Algorithms (GA)

The use of all these 86 features (attributes) is impractical for change detection since some unrelated features may cause errors in classifying land-use types. In addition, the classification will involve high dimensional data if all of these features are used. Some data compression techniques, such as principal components analysis (PCA), could be used to reduce the data volume. However, PCA transforms data based on variances; thus, unrelated information may be included in the transformation. Moreover, the meanings of the transformed variables cannot be easily understood.

An alternative is to select the optimal subset of features based on heuristic search programs. A genetic algorithm (GA) can be used to facilitate the selection of the optimal subset of features for land-use classification. The optimization procedure of GA is devised by simulating the natural selection process in biology (Goldberg, 1989; Mitchell, 1996). The mechanism of creating a better generation is based on the adaptation of individuals. Fitness functions are used to indicate the performance of each solution or individual (chromosome) in solving the optimal problem. This evolution process is repeated until some conditions are satisfied or the best solution is found. The best fit (elite) individual will be an optimum or close to the optimum solution.

The optimal set of *N* features should be determined so that land-use types can be best discriminated between these objects. The discrimination is based on the Euclidian distance:

$$SIM^{t_i}(i,j) = \sqrt{\sum_{m=1}^{N} w_m (a_{im} - a_{jm})^2} \qquad (1)$$

where $SIM^{t_i}(i,j)$ is the similarity (distance) between objects *i* and *j* in terms of the normalized attribute a ($a \in (0,1)$) t a time t_i, *N* is the total number of attributes, and w_m is the weight for the mth attribute with $w_m = 0$ or 1 (1 for selected features and 0 for non-selected features).

Since the change detection is based on time series of the SAR images (from t_1 to t_n), the accumulative distance is used:

$$SIM^{t_1,t_n}(i,j) = \sum_i SIM^{t_i}(i,j). \qquad (2)$$

where $SIM^{t_1,t_n}(i,j)$ is the accumulative distance from t_1 to t_n.

The total distances of all objects within each land-use class and between these classes can be then calculated by using these features. A fitness function is therefore defined according to the ratio of these two distances:

$$F(x) = \frac{\sum_{\omega_i = \omega_j} SIM^{t_1,t_n}(i,j)}{\sum_{\omega_i \neq \omega_j} SIM^{t_1,t_n}(i,j)} \qquad (3)$$

where ω is the land-use class.

A lower value of $F(x)$ indicates that the difference is smaller within a class and larger between classes. The objective is to minimize the value of $F(x)$ so that the land-use classes can be best discriminated. The possible combinations of the subsets are enormous, and GA is an excellent method for quickly finding an approximate global minimum value according to the fitness function.

In the programming, the population size of GA was set to 100. The crossover rate and the mutation rate were 0.90 and 0.01, respectively. The strategies of elitist selection and diversity operation were also used to facilitate the search for the optimal parameters. The GA program was able to identify the optimal set of these selected features according to the evolutionary approach. The training data (actual land-use types) were collected by using field investigation for the training of GA (Table 2). A commercial genetic algorithm package, GeneHunter, was used to implement the feature selection process.

The GA optimization found that the use of the following eight features could generate the largest value of the fitness function:

- Average backscattering coefficient (*Mean*) calculated from backscattering coefficient (c_i) of all *n* pixels of each segmented image object. $Mean = \frac{1}{n} \sum_{i=1}^{n} c_i$;
- The maximum backscattering coefficient (*Max*) of each segmented image object. $Max = \max(c_i, i \in 1 \ldots n)$;
- Ratio to scene in terms of backscatter, which means the mean backscattering coefficient value of an image object divided by the mean value of the whole scene. $r = \frac{Mean_{object}}{Mean_{scene}}$;
- Grey-level co-occurrence matrix (GLCM) dissimilarity. $GLCM\_Dissimilarity = \sum_{i,j=0}^{M-1} P_{i,j} |i - j|$, where *i* is the row number and *j* is the column number in the texture calculation cell matrix, $P_{i,j}$ is the normalized value in cell *i* and *j*, *M* is the number of rows or columns of cell matrix, and $P_{i,j} = \frac{V_{i,j}}{\sum_{i,j=0}^{M-1} V_{i,j}}$, $V_{i,j}$ is the value in the cell *i* and *j* of the image window;

- GLCM mean is the average value in terms of the GLCM.

$$GLCM\_Mean = \frac{\sum\limits_{i,j=0}^{N-1} P_{i,j}}{N^2};$$

- GLCM correlation measures the linear dependency of grey levels of neighboring pixels. $GLCM\_Correlation =$

$\sum\limits_{i,j=0}^{M-1} P_{i,j} \left[\dfrac{(i - \mu_i)(j - \mu_j)}{\sqrt{(\sigma_i^2)(\sigma_j^2)}} \right]$, where μ_i is the average value in row i and μ_j is the average value in column j, σ_i is the standard deviation of row i and σ_j is the standard deviation of column j;

- GLCM homogeneity measures the local homogenous of the cell matrix. $GLCM\_Homogeneity = \sum\limits_{i,j=0}^{M-1} \dfrac{P_{i,j}}{1 + (i - j)^2}$; and

- GLCM entropy is high if the GLCM is distributed equally: $GLCM\_Entropy = \sum\limits_{i,j=0}^{M-1} P_{i,j}(- \ln P_{i,j}).$

Incorporating Case-based Reasoning for Change Detection

Establishing the Case Library for Change Detection

The case library stores the discrete cases that represent the knowledge for change detection. A case is a contextualized piece of knowledge representing an experience that can help a reasoner achieve his/her goals (Kolodner, 1993). The basic unit of cases is the derived objects (land parcels) from the object-oriented analysis. A case consists of two parts: the description of the problem (e.g., backscatter properties and other object attributes of a land parcel) and the solution to the problem (e.g., the land-use classes or change classes). However, it is impractical to include the information of change classes directly in each case because the number of change classes is very large. For example, the possible change classes will be 100 if there are 10 land-use classes. In this study, the solution to the problem is represented by land-use classes instead of change classes.

A case, which is related to a land parcel (object), is defined as follows:

$$c = \{x_1^i, x_2^i, \ldots, x_n^i; y^i\} \tag{4}$$

where x_j^i is description attribute j (e.g., backscatters and other object attributes) of land parcel i, and y^i is the solution attribute (land-use type) of the land parcel.

The description attributes include both spectral information (backscatters) and object-oriented information (textural

and shape properties). The solution attribute is the land-use class. The cases are selected through field investigations with the assistance of GPS (Table 2). These cases are distributed across typical land-use classes based on stratified random sampling (Congalton, 1991). Since the reasoning is related to the temporal dimension, the case is further represented by the following form:

$$C^T = \{X_1^{iT}; X_2^{iT}; X_3^{iT}; \cdots, X_n^{iT}; Y^{iT}\} \tag{5}$$

where X_j^{iT} is description attribute j of case i during period T (t to $t + $ n), and Y^{iT} is the solution attribute (land-use type) of case i.

The cases in the case library are collected over land parcels that have not experienced land-use changes (stable land-use). A land-use class is represented by a group of cases. These cases are discrete because a case may be quite different from others within the same class. The use of discrete cases can help to reflect the heterogeneity of a land-use class. This provides much more flexibility in representing the complex relations between the variables (description attributes) and land-use classes. Statistical methods may not be suitable for capturing complex relationships. For example, the backscatter variation of a land-use class due to wetness changes is difficult to consider with conventional statistical methods.

Table 4 shows the typical backscatter behaviors of some land-use types. The backscatter was obtained from the Radarsat images after they had been calibrated. The known land-use types were obtained from field work. Built-up areas were found to have the largest backscatter ($-0.27 \sim 3.16$), while water had the lowest ($-9.42 \sim -10.74$). Forests had seasonal changes in terms of backscatter, such as the lowest value in January. Paddy fields had the lowest value of backscatter in March when they are inundated. Other agricultural lands had periodic changes (3 to 4 months) of backscatter as a result of the growth cycle.

A CBR-based Matching Algorithm for Change Detection

After the case library has been established, case matching is carried out to determine the land-use class for an unknown case (land parcel). The matching is based on the similarity between an input (questioned) case and a known case in the case library. These similarities can locate the queried case i to its nearest known case j in the library. It assumes that the land-use class of the queried case will be the same as that of its nearest neighbor (a known case). The known case has a target function of $\eta(j)$ (e.g., indicating its land-use class). This reasoning assumes that the case closest to j tends to

TABLE 4. TYPICAL BACKSCATTERS FOR VARIOUS LAND-USE TYPES IN THE STUDY AREA

Time Type	2005						2006								
	29 Sep	23 Oct	16 Nov	10 Dec	03 Jan	27 Jan	20 Feb	16 Mar	09 Apr	03 May	27 May	20 Jun	14 Jul	07 Aug	31 Aug
River	−24.6	−24.3	−23.8	−23.6	−23.7	−20.4	−21.1	−21.5	−20.0	−21.1	−20.2	−21.9	−19.9	−22.0	−21.8
Fishpond	−21.5	−20.8	−20.5	−20.1	−19.6	−17.1	−16.4	−17.0	−16.2	−9.8	−10.6	−11.0	−8.8	−7.8	−7.3
Paddy	−11.4	−10.8	−11.3	−11.3	−11.4	−9.5	−8.6	−8.7	−8.2	−6.8	−7.7	−8.6	−10.2	−9.5	−7.3
Bare land	−6.6	−8.5	−8.3	−8.9	−7.6	−5.2	−3.0	−2.5	−2.6	−0.9	−1.9	−2.7	−1.8	−3.3	−3.3
Rural residential	−5.0	−5.9	−5.8	−5.4	−5.5	−3.6	−3.7	−3.8	−2.8	−3.5	−2.5	−4.4	−3.8	−4.1	−4.5
Built-up	−1.4	−2.6	−2.0	−2.5	−1.9	0.5	1.1	0.6	1.2	1.5	2.5	1.3	0.6	1.5	−0.2
Vegetable land	−7.8	−9.2	−9.1	−9.4	−10.1	−8.3	−7.4	−7.6	−6.1	−5.9	−5.6	−6.1	−6.9	−6.0	−7.2
Forest	−9.8	−10.8	−10.6	−10.5	−10.6	−9.4	−9.4	−9.2	−7.9	−7.8	−7.4	−7.8	−7.8	−8.1	−8.3
Orchard	−5.8	−8.9	−9.3	−9.0	−8.7	−7.2	−5.8	−6.0	−5.1	−4.8	−3.8	−3.6	−3.7	−3.2	−4.5

have a target function close to $\eta(j)$. Actually, CBR often adopts the most popular k-Nearest Neighbors (k-NN) for reasoning. The k-NN algorithm can work well on many practical problems and is fairly noise tolerant in CBR applications (Dasarathy, 1991).

Intuitively, the k-NN algorithm assigns to each new queried case the majority class (state) among its k nearest neighbors, which are determined by the accumulative similarity. For a discrete value of $\eta(j)$, this k-NN algorithm is represented as follows (Dasarathy, 1991; Houben *et al.*, 1995):

$$\hat{\eta}(i) \leftarrow \operatorname*{argmax}_{s \in S} \sum_{j=1}^{k} \delta(s,\eta(j)) \begin{cases} \delta(s,\eta(j)) = 1, & if \quad s = \eta(j) \\ \delta(s,\eta(j)) = 0, & if \quad s \neq \eta(j) \end{cases} \quad (6)$$

where k is the total number of nearest neighbors, and s is the finite set of target class values. In this study, it represents various land-use types, such as orchard, forest, and water.

This equation assumes that each neighbor has the same vote on determining land-use class. A better way is to address the fact that a closer neighbor should have greater influence than others in the reasoning. A distance-weighted function can be incorporated in the k-NN algorithm (Jia and Richards, 2005):

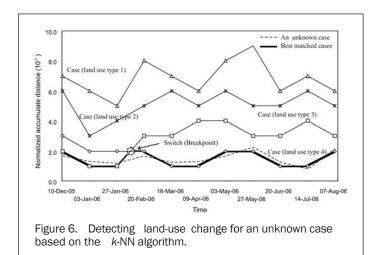$$\hat{\eta}(i) \leftarrow \operatorname*{argmax}_{s \in S} \sum_{j=1}^{k} w_{fj} \cdot \delta(s,\eta(j)). \quad (7)$$

These feature-distance-weights (w_{fj}) are proportional to the inversed accumulative similarity:

$$w_{fj} = \frac{1}{SIM^{t_1,t_n}(i,j))^2} \quad (8)$$

where $\hat{\eta}(i) = \eta(j) \quad if \quad SIM(i,j) = 0$

The algorithm matches an unknown case (object) to the known cases according to the accumulative similarity. The accumulative similarity, $SIM^{t_1,t_n}(i,j)$, in Equation 2 is calculated from multi-temporal data. The accumulative similarity is normalized within 0 and 1 for better comparison.

An unknown case without land-use changes will be associated with one single land-use type for the whole time according to these similarities. Therefore, land-use changes can be identified if this case is associated with two or more land-use types at different times. Figure 6 illustrates that land-use changes can be conveniently

detected by using the proposed matching algorithm. An unknown case will be matched with the known cases in the library (e.g., the four cases). This unknown case is matched with case 3 in the first period and case 4 in the second period based on the minimal normalized accumulative similarity (the k-NN algorithm). The switch point between these two matched curves represents the temporal position at which land-use change took place. Figure 6 shows that a land parcel (object) experienced the change from land-use type 3 to land-use type 4 between 27 January 2006 and 20 February 2006.

The detailed procedures for detecting the temporal positions (breakpoints) of land-use changes are described as follows:

1. Calculating the accumulative similarities, $SIM^{t_1,t_i}(x,C)$ and $SIM^{t_1,t_i+1}(x,C)$, between an unknown case (x) and all the known cases (C) in the case library according to equation 2;
2. Assigning land-use classes, x, $\omega^{t_i}(x)$ and $\omega^{t_{i+1}}(x)$, to the unknown case x for t_i and t_i+1 based on the best match using the k-NN algorithm described by Equation 7; and
3. Identifying the switch point (temporal breakpoint) if an unknown case is associated with two or more land-use classes ($\omega^{t_i}(x) \neq \omega^{t_{i+1}}(x)$).

Results of Change Detection and Validation

The initial land-use map of the study area should be obtained before using the multi-temporal Radarsat images for change detection. The map can be obtained from either survey or remote sensing classification. The first option seems to be infeasible because there are difficulties in updating survey maps on a monthly basis. For the second option, there are still some difficulties in obtaining the updated land-use map from optical remote sensing. Radarsat images that have only one single polarization (HH polarization) and one single band (C-band) could produce much confusion in land-use classification. One compromise is to use multi-temporal Radarsat images. The proposed matching algorithm needs at least three multi-temporal SAR images for curves (cases) matching to determine land-use types. Therefore, in this study the initial land-use (dated on 16 November 2005) was obtained by using three dates of Radarsat images dated on 20 September 2005, 23 October 2005, and 16 November 2005.

Table 5 gives the errors of the initial land-use classification. The overall error is 21.1 percent for the initial land-use classification with just three times at C-band. Land-use classification has the inherent problem of serious confusions with the use of single-band SAR images (Li and Yeh, 2004). However, this problem could be alleviated for change detection analysis. The following analysis will show that the accuracy of the change detection will be slightly better than the classification accuracy.
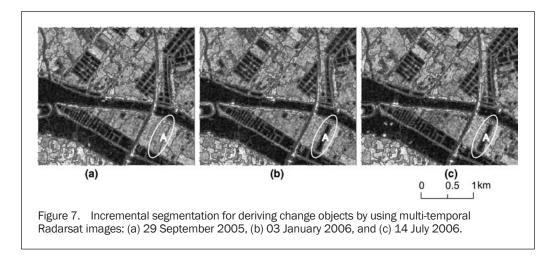

Figure 6. Detecting land-use change for an unknown case based on the k-NN algorithm.

TABLE 5. ACCURACIES OF THE INITIAL LAND-USE CLASSIFICATION USING MULTI-TEMPORAL RADARSAT IMAGES

Land-use types	Classification error (%)
built-up areas	19.7
rural residential areas	15.6
bare land	24.9
vegetable land	29.8
paddy fields	15.9
orchards	27.5
forest	23.0
river	7.9
fishpond	15.1
Overall accuracy	*21.1*

Land-use changes at monthly intervals were then obtained by using the proposed CBR matching algorithm. The change detection was based on object-oriented rather pixel-oriented methods. Figure 7 illustrates that the incremental segmentation can effectively derive change objects (e.g., Location *A*). Figure 8a shows the progress of the Zhujiang Development Project at Location *A*, which was in the ground clearance phase in November 2005, the construction phase in February 2006, and the completion phase in May 2006.

Table 6 shows the normalized accumulative similarity for various land-use types at Location *A* based on Equation 2. The smallest value indicates the best matched land-use type. The matching indicates that this site was converted from bare land to a built-up area. Actually, it was completely converted from development land (bare land) to built-up land on 16 March 2006 (Table 6). The development process can be effectively monitored according to the change in the matched land-use types.

Situated in the Pearl River Delta, the study area has a long history of fish farming. In the past, however, land-use was mainly restricted to paddy production for securing food supply under the planning economy. After the economic reform, a significant amount of agricultural land was converted into fishponds to obtain higher economic returns. This conversion consisted of four steps: land clearance, digging, drying, and recharging with water. These processes can be monitored using sequential SAR images. Figure 8b shows the identified new fishponds at location *A* by using these multi-temporal SAR images. According to the similarity matching algorithm, the site was identified as an orchard in September 2005, but as cleared land (bare land) in January 2006, and then inundated land in May 2006. Figure 8b also clearly shows that a fishpond site experienced some seasonal changes at location *B*. It was always inundated land, except that it was discharged with water in January 2006. It was recharged with water again after the digging.
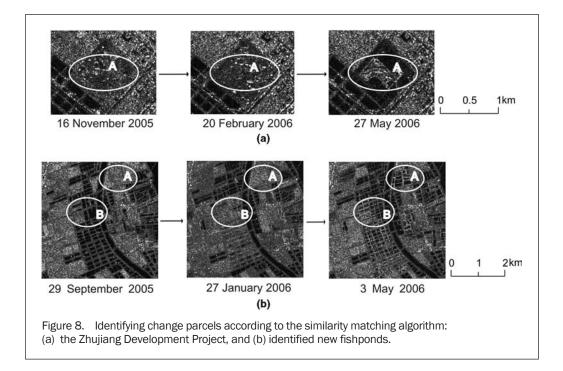

Figure 7. Incremental segmentation for deriving change objects by using multi-temporal Radarsat images: (a) 29 September 2005, (b) 03 January 2006, and (c) 14 July 2006.

Figure 8. Identifying change parcels according to the similarity matching algorithm: (a) the Zhujiang Development Project, and (b) identified new fishponds.

	River	Fishpond	Paddy	Vegetable	Orchard	Forest	Bare land	Built-up	Rural residential
	Normalized accumulative distance								
10 Dec 2005	0.006	0.004	0.005	0.003	0.015	0.002	**0.001**	0.003	0.003
03 Jan 2006	0.004	0.003	0.004	0.003	0.014	0.009	**0.001**	0.002	0.002
27 Jan 2006	0.010	0.011	0.003	0.008	0.013	0.019	**0.002**	0.006	0.004
20 Feb 2006	0.008	0.006	0.003	0.004	0.015	0.016	**0.002**	0.007	0.004
16 Mar 2006	0.003	0.007	0.003	0.003	0.014	0.020	0.002	**0.001**	0.002
09 Apr 2006	0.007	0.004	0.003	0.003	0.014	0.014	0.002	**0.002**	0.002
03 May 2006	0.002	0.007	0.009	0.004	0.015	0.023	0.002	**0.002**	0.003
27 May 2006	0.008	0.019	0.008	0.005	0.019	0.017	0.003	**0.002**	0.003
20 Jun 2006	0.009	0.006	0.004	0.013	0.012	0.014	0.006	**0.002**	0.003
14 Jul 2006	0.005	0.005	0.003	0.009	0.011	0.010	0.005	**0.001**	0.002
07 Aug 2006	0.003	0.002	0.005	0.013	0.010	0.011	0.004	**0.001**	0.002
31 Aug 2006	0.009	0.006	0.004	0.012	0.009	0.008	0.005	**0.002**	0.002

Plate 1 and Table 7 are the detection results in terms of temporal positions and the kind of changes. A large part of the changes involves the conversion from one type of agricultural land-use to another, such as from vegetable land to orchard, vegetable land to paddy fields, orchard to vegetable land, or paddy to vegetable land. This conversion reflects the rotation of agricultural activities in this region. Traditional optical remote sensing cannot monitor these detailed monthly changes in this sub-tropical region. This study reveals some change patterns that are related to the crop calendar. For example, there are a greater number of changes from vegetable land to paddy fields in February, which is the season for planting paddy. The conversion from vegetable land to orchard mainly takes place in February and March, which are the months for growing banana and sugarcane. However, land development can take place in any season. Multi-temporal SAR images can identify the three stages of land development: (a) vegetated land, (b) land cleared for construction (bare land), and (c) completion as built-up areas.

The validation of the change detection was carried out by comparing this proposed method with other common methods. There are four possible combinations of change detection methods, object-based or pixel-based plus case-based or rule-based. It is expected that object-based is better than pixel-based for change detection because of using ancillary object features. Case-based is also better than rule-based because the former has a strong capability for capturing complex patterns of land-use changes (Mcsherry, 1998; Cunningham *et al.*, 2003; Roth-Berghofer, 2004). Therefore, compared with the other three methods, the proposed method of object-based plus case-based should be the optimal combination for change detection by using multi-temporal SAR data.

The rule-based method (Quinlan, 1986; Quinlan, 1990) and the pixel-based method (Li and Yeh, 2004) were tested in this study. In the rule-based method, classification rules were extracted by using SEE5 (Windows version), which is a common data mining software developed by RuleQuest Company. The classification was implemented in ERDAS by using the extracted rules. The main differences between pixel-based classification and object-based classification are the unit of training data and the attributes used for classification. The training data of pixel-based classification is the information of a pixel (backscatter coefficient) and its corresponding land-use type, while the training data of object-based classification is the spectrum and texture information (e.g., backscatter coefficient and GLCM_Dissimilarity) of a object (land parcel), and its corresponding land-use type. Therefore, many more attributes are used in object-based classification.

The accuracy of these methods were assessed by using the validation data (Table 2). Table 8 shows the accuracies of detecting the main types of land-use conversion using these methods. It was found that the proposed method (the combination of the object-based and case-based methods) had the best performance with the lowest overall error (14.1 percent). The conventional method (the combination of the pixel-based and rule-based method) has the poorest performance with the largest overall error (23.0 percent). Generally, these two change classes, the Vegetable to Orchard class and the Orchard to Vegetable class, have larger overall errors. The changes related to water (e.g., Fishpond to Vegetable) usually have the lowest errors because of the unique backscatters of water.

In Table 8, the accuracy of the Vegetable to Orchard class was identified with an overall error of 13.5 percent, while the Orchard to Vegetable class was identified with an overall error of 22.9 percent. Similarly, the Forest to Vegetable class was identified with an overall error of 23.3 percent. These accuracies seem to be unusual because these latter two classes should be comparatively easy to discern (as they involve complete tree removal). There are three reasons for explaining these exceptions. First, the Vegetable to Orchard class mainly represents the conversion from vegetables to banana or sugar canes. These changes are quite common in the study area. Second, the Forest to Vegetable class is often confused with the Forest to Bare land class after the removal. Third, the Forest to Vegetable class has a very small chance of taking place in the study area. The collected cases in the case library may not well capture the knowledge. This may result in the larger error observed.

The same explanations are applied to the accuracies for Forest to Bare land class and Vegetable to Bare land class. The former should be much easier to discern than the latter. However, the former is quite rare in the study area. The accuracy for detecting it is reduced because of the fewer known cases available for the reasoning.

Some confusion in the change detection of this study may arise from the Radarsat radar frequency (i.e., C-band), which has poor penetration capability. In future work, multi-temporal L-band SAR data could be used to improve land-use change detection by using the proposed method.

Conclusions

Radar remote sensing is attractive for monitoring rapid land-use changes because it is not affected by cloud cover
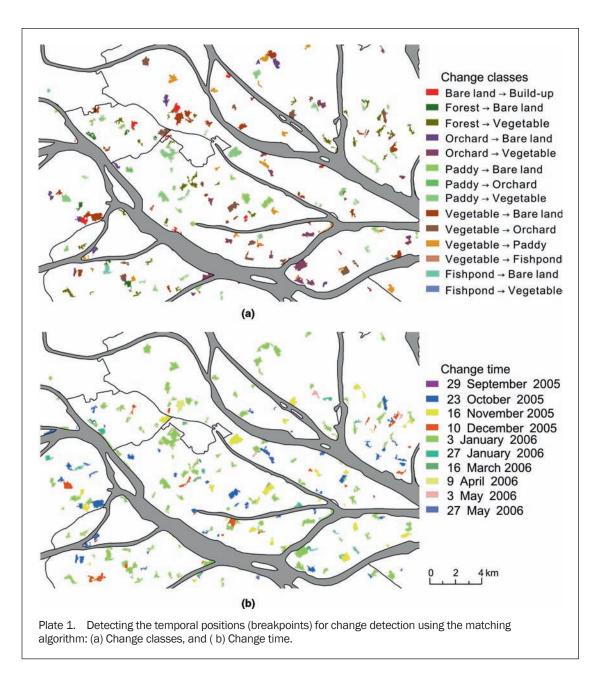
Plate 1. Detecting the temporal positions (breakpoints) for change detection using the matching algorithm: (a) Change classes, and (b) Change time.

TABLE 7. MAJOR TYPES OF LAND-USE CHANGES (KM^2) IN THE STUDY AREA USING THE PROPOSED METHOD

Change Classes \ Time	10 Dec 2005	03 Jan 2006	27 Jan 2006	20 Feb 2006	16 Mar 2006	09 Apr 2006	3 May 2006	27 May 2006	20 Jun 2006	14 Jul 2006	07 Aug 2006	31 Aug 2006
Bare land to Built-up	2.06	1.60	2.59	1.98	2.26	1.20	5.32	9.93	6.36	4.37	5.92	5.46
Forest to Bare land	0.97	10.62	0.90	3.39	0.36	0.88	0.94	0.97	1.40	0.80	0.09	2.55
Forest to Vegetable	1.71	1.97	0.63	0.87	0.51	0.88	0.07	1.03	0.13	0.11	0.89	0.60
Orchard to Bare land	0.00	0.22	0.00	0.09	0.06	0.35	0.00	0.00	0.00	0.00	0.00	0.00
Orchard to Vegetable	3.94	13.11	8.41	9.63	8.27	12.75	14.83	6.27	9.51	10.27	4.96	8.19
Paddy to Bare land	0.00	0.54	0.19	0.83	0.62	0.16	0.03	0.07	0.29	0.06	0.03	0.33
Paddy to Orchard	0.29	0.24	0.72	1.20	0.81	1.47	0.60	3.16	0.34	1.63	3.48	3.45
Paddy to Vegetable	3.22	6.17	5.17	3.88	6.11	5.43	4.53	1.66	3.00	4.44	1.74	5.33
Vegetable to Bare land	0.41	8.89	1.99	9.31	10.73	4.56	0.38	0.94	1.15	3.00	0.06	2.15
Vegetable to Orchard	0.39	0.00	0.00	0.21	0.00	0.11	0.02	0.05	0.00	0.21	0.09	0.11
Vegetable to Paddy	2.74	7.43	4.54	0.05	0.19	0.00	2.48	9.16	6.00	1.92	5.65	8.53
Vegetable to Fishpond	0.29	0.83	0.50	0.90	1.25	1.87	0.99	2.26	1.77	3.27	0.88	2.31
Fishpond to Bare land	0.91	1.39	0.55	0.59	0.10	0.24	0.24	0.61	0.12	0.11	0.18	0.36
Fishpond to Vegetable	1.04	0.64	1.52	1.28	1.43	1.04	2.26	1.28	1.99	4.46	1.75	5.35

	Change Classes	Case-based			Rule-based		
		False alarms	Missed alarms	Overall errors (%)	False alarms	Missed alarms	Overall errors (%)
Pixel-based	Bare land to Built-up	11.8	9.5	21.3	11.5	10.8	22.3
	Forest to Bare land	12.5	10.9	23.4	13.2	10.6	23.8
	Forest to Vegetable	15.2	14.5	29.7	15.5	14.4	29.9
	Orchard to Bare land	13.7	10.9	24.6	13.5	9.5	23.0
	Orchard to Vegetable	14.5	15.2	29.7	14.8	15.7	30.5
	Paddy to Bare land	12.8	11.2	24.0	10.3	12.1	22.4
	Paddy to Orchard	12.0	10.9	22.9	12.1	11.3	23.4
	Paddy to Vegetable	14.5	12.9	27.4	15.1	10.7	25.8
	Vegetable to Bare land	12.3	10.8	23.1	12.6	8.8	21.4
	Vegetable to Orchard	14.6	14.9	29.5	15.5	14.1	29.6
	Vegetable to Paddy	11.8	10.4	22.2	12.9	10.4	23.3
	Vegetable to Fishpond	12.4	9.7	22.1	15.4	11.3	26.7
	Fishpond to Bare land	9.9	13.8	23.7	12.4	10.9	23.3
	Fishpond to Vegetable	12.8	10.7	23.5	14.8	12.8	27.6
	Average	*12.9*	*11.9*	*24.8*	*13.5*	*11.7*	*25.2*
Object-based	Bare land to Built-up	6.8	5.8	12.6	9.4	8.1	17.5
	Forest to Bare land	7.3	5.9	13.2	9.9	8.7	18.6
	Forest to Vegetable	12.8	10.5	23.3	8.5	6.4	14.9
	Orchard to Bare land	9.3	6.7	16.0	14.5	10.4	24.9
	Orchard to Vegetable	12.6	10.3	22.9	13.8	11.7	25.5
	Paddy to Bare land	6.9	6.3	13.2	9.5	10.8	20.3
	Paddy to Orchard	9.1	7.9	17.0	9.8	8.9	18.7
	Paddy to Vegetable	8.8	6.4	15.2	11.1	10.1	21.2
	Vegetable to Bare land	7.4	5.8	13.2	10.8	9.7	20.5
	Vegetable to Orchard	6.6	6.9	13.5	9.5	9.1	18.6
	Vegetable to Paddy	6.8	6.3	13.1	10.2	9.9	20.1
	Vegetable to Fishpond	5.4	5.4	10.8	13.4	9.7	23.1
	Fishpond to Bare land	7.5	4.9	12.4	10.8	9.6	20.4
	Fishpond to Vegetable	7.9	5.3	13.2	11.9	10.2	22.1
	Average	*8.2*	*6.7*	*15.0*	*10.9*	*9.5*	*20.5*

and other weather conditions. Elaborated techniques should be developed by using time-series SAR images for monitoring short-interval land-use changes. This paper has demonstrated that a number of techniques, such as object-based analysis and case-based reasoning, can help to improve the performance of land-use change detection. A major problem of using object-based analysis for multi-temporal SAR images is the exponential increase of patches if more sequential images are included in the change detection. An incremental segmentation procedure can be used to reduce the possibility of fragmented object delineation in temporal images. It can effectively generate two types of homogenous objects (land parcels): stable objects without land-use changes and objects with land-use changes.

A total of 86 features were derived from the object-based analysis. Feature selection is necessary for producing effective change detection by using this ancillary information. The feature selection based on GA only identifies the eight optimal features for the best discrimination of land-use types. These selected features are the average backscattering coefficient, the maximum backscattering coefficient, the ratio to scene in terms of backscatter, the grey-level co-occurrence matrix (GLCM), the GLCM mean, the GLCM correlation, the GLCM homogeneity, and the GLCM entropy. These object-based features are treated as the independent variables for inferring land-use changes.

The aim of this proposed method is to identify the temporal positions and the kind of changes by using the case-based reasoning method. The accumulative similarity is defined by using multi-temporal SAR images. A matching algorithm is proposed to examine whether an object is associated with two or more land-use types in the temporal dimension by using the accumulative similarity. Discrete cases are used to capture the complex relationship between the independent variables and land-use changes.

The experiments have demonstrated that monthly activities (e.g., rotation of crops and land development) can be effectively monitored with the proposed method. The change patterns of the study area can be revealed according to the matching algorithm. For example, different stages of land development (clearance, construction, and full conversion to built-up areas) can be identified in multi-temporal SAR images. The monitoring of short-term land-use changes is required for a fast growing region that has a lot of illegal land developments. Short-term monitoring can help to prevent illegal development at an early stage.

Comparisons of pixel-based versus object-based and case-based versus rule-based methods were made to test their effectiveness for change detection. The analysis indicates that the proposed method (a combination of object-based and case-based methods) can yield the lowest overall error of change detection (14.1 percent). The conventional method (a combination of pixel-based and rule-based methods) has the largest overall error (23.0 percent). The proposed method can significantly improve on the accuracy

of the conventional method by 8.9 percentage points, that is, 85.9 percent compared with 77.0 percent.

Time series analysis for change detection is still quite a complicated problem. Change detection using temporal remote sensing images requires a good understanding of the background environment and intelligent reasoning. Conventional methods are not effective for identifying the time breakpoint when land-use changes take place In contrast, the proposed CBR matching algorithm seems to provide a convenient and practical solution to the detection of land-use changes in the spatio-temporal dimensions by using multi-temporal SAR data.

Further studies are needed to apply the proposed method to other sources of SAR images when they are available. Although current orbital radar platforms are limited to a single acquisition frequency, advanced sensors such as the ALOS/PALSAR have dual- and quad-polarimetric modes. Future studies should incorporate polarimetric information for improving land-use classification and change detection. Moreover, multi-temporal L-band SAR data with better penetration capability can also be used to discriminate land-use types more effectively.

Acknowledgments

References

Baatz, M., and A. Schäpe, 2000. Multiresolution segmentation - An optimization approach for high quality multi-scale image segmentation, *Angewandte Geographische Informationsverarbeitung*, 12:12–23.

Baatz, M., U. Benz, S. Dehghani, M. Heynen, A. Höltje, P. Hofmann, I. Lingenfelder, M. Mimler, M. Sohlbach, and M. Weber, 2004. *eCognition Professional User Guide 4*, Definiens Imaging, Munich.

Baghdadi, N., M. Bernier, R. Gauthier, and I. Neeson, 2001. Evaluation of C-band SAR data for wetlands mapping, *International Journal of Remote Sensing*, 22:71–88.

Benz, U.C., P. Hofmann, G. Willhauck, I. Lingenfelder, and M. Heynen, 2004. Multi-resolution, object-oriented fuzzy analysis of remote sensing data for GIS-ready information, *ISPRS Journal of Photogrammetry and Remote Sensing*, 58:239–258.

Bovolo, F., and L. Bruzzone, 2005. A detail-preserving scale-driven approach to change detection in multitemporal SAR images, *IEEE Transactions on Geoscience and Remote Sensing,* 43(12):2963–2972.

Branting, K.L., and J.D. Hastings, 1994. An empirical evaluation of model-based cased matching and adaptation, *Proceedings of the American Association for Artificial Intelligence, Case-based Reasoning Workshop*, Seattle, Washington, pp. 72–78.

Champagne, C., H. Mcnair, and J. Shang, 2006. An object-oriented approach to land-use mapping in the Canadian Prairies, *Proceedings of the Eleventh Biennial USDA Forest Service Remote Sensing Applications Conference*, Salt Lake City, Utah.

Chubey, M., S. Franklin, and M. Wulder, 2006. Object-based analysis of Ikonos-2 imagery for extraction of forest inventory parameters, *Photogrammetric Engineering & Remote Sensing*, 72(4):383–394.

Congalton, R.G., 1991. A review of assessing the accuracy of classification of remotely sensed data, *Remote Sensing of Environment*, 37:35–46.

Cunningham, P., D. Doyle, and J. Loughrey, 2003. An evaluation of the usefulness of case-based explanation, *Lecture Notes in Computer Science*, 2689:22–130.

Dasarathy, B.V., 1991. Nearest neighbor (NN) norms: NN pattern classification techniques, *IEEE Computer Society Press*, Los Alamitos, California, 447 p.

Dobson, M.C., L.E. Pierce, and F.T. Ulaby, 1996. Knowledge-based land cover classification using ERS-1/JERS-1 SAR composites, *IEEE Transactions on Geoscience and Remote Sensing*, 34:83–99.

Eastman, J.R., and M. Fulk, 1993. Long sequence time series evaluation using standardized principal components, *Photogrammetric Engineering & Remote Sensing*, 59(8):1307–1312.

Goldberg, D.E., 1989. *Genetic Algorithms in Search, Optimisation and Machine Learning*, Addison-Wesley, Reading, Massachusetts, pp. 412.

Grund, M.C., 2003. *The Automated Segmentation of Synthetic Aperture Radar Imagery*, UMI ProQuest Digital Dissertations, University of Nevada, Reno, pp. 96–100.

Houben, I., L. Wehenkel, and M. Pavella, 1995. Coupling of K-NN with decision trees for power system transient stability assessment, *Proceedings of the 4ᵗʰ IEEE Conference*, pp. 825–832.

Howarth, P.J., and G.M. Wickware, 1981. Procedures for change detection using Landsat digital data, *International Journal of Remote Sensing*, 2(3):277–291.

Huang, X.Q., and J.R. Jensen, 1997. A machine-learning approach to automated knowledge-base building for remote sensing image analysis with GIS data, *Photogrammetric Engineering & Remote Sensing*, 63(10):1185–1194.

Jia, X.P., and J.A. Richards, 2005. Fast k-NN classification using the cluster-space approach, *IEEE Geoscience and Remote Sensing Letters*, 2(2):225–228.

Kolodner, J., 1993. *Case-based Reasoning*, Morgan Kaufmann, San Mateo, California, pp. 668.

Langford, W.T., 2002. *Evaluation Functions in Aerial Image Segmentation*, UMI Proquest Digital Dissertations, Oregon State University, Corvallis, Oregon, pp. 50–84.

Lekkas, G.P., N.M. Avouris, and L.G. Viras, 1994. Case-based reasoning in environmental monitoring applications, *Applied Artificial Intelligence, An International Journal*, 8:359–376.

Li, X., and A.G.O. Yeh, 1998. Principal component analysis of stacked multi-temporal images for the monitoring of rapid urban expansion in the Pearl River Delta, *International Journal of Remote Sensing*, 19(8):1501–1518.

Li, X., and A.G.O. Yeh, 2004. Multitemporal SAR images for monitoring cultivation systems using case-based reasoning, *Remote Sensing of Environment*, 90(4):524–534.

Lopes, A., E. Nezry, R. Touzi, and H. Laur, 1993. Structure detection and statistical adaptive speckle filtering in SAR images, *International Journal of Remote Sensing*, 14(9):1735–1758.

Magagi, R., M. Bernier, and C.H. Ung, 2002. Quantitative analysis of RADARSAT SAR data over a sparse forest canopy, *IEEE Transactions on Geoscience and Remote Sensing*, 40:1301–1313.

Mcavoy, J.G., and E.M. Krakowski, 1989. A knowledge based system for the interpretation of SAR images of sea ice, *International Geoscience and Remote Sensing Symposium (IGARSS'89)*, 2:844–847.

Mcsherry, D., 1998. An adaptation heuristic for case-based estimation, *Lecture Notes in Computer Science*, 1488:184–195.

Mitchell, M., 1996. *An Introduction to Genetic Algorithms*, MIT Press, Cambridge, Massachusetts, pp. 205.

Pierce, L.E., K.M. Bergen, M.C. Dobson, and F.T. Ulaby, 1998. Multitemporal land-cover classification using SIR-C/X-SAR imagery, *Remote Sensing of Environment*, 64:20–33.

Quinlan, J.R., 1986. Introduction of decision trees, *Machine Learning*, 1:81–106.

Quinlan, J.R., 1990. Decision trees and decision-making, *IEEE Transactions on Systems, Man and Cybernetics*, 20(2):339–346.

Ranson, K.J., and G. Sun, 2000. Effects of environmental conditions on boreal forest classification and biomass estimates with SAR, *IEEE Transactions on Geoscience and Remote Sensing*, 38:1242–1252.

Richards, J.A., and X.P. Jia, 1999. *Remote Sensing Digital Image Analysis: An Introduction*, Springer, New York, pp. 362.

Roth-Berghofer, T., 2004. Explanations and case-based reasoning: Foundational issues, *Lecture Notes in Computer Science*, 3155:389–403.

Uchiyama, T., and M.A. Arbib, 1994. Color image segmentation using competitive learning, *IEEE Transactions on Pattern Analysis and Machine Intelligence*, 16(12):1197–1206.

Watson, I., 1997. *Applying Case-Based Reasoning: Techniques for Enterprise Systems*, Morgan Kaufmann Publishers, Inc, California, pp. 245.

Yeh, A.G.O., and X. Shi, 1999. Applying case-based reasoning to urban planning: A new planning-support system tool, *Environment and Planning B*, 26(1):101–115.